Electronic Supplementary Material (ESI) for Dalton Transactions.

Two [Ln_4] molecular rings folded as compact tetrahedra

Jorge Salinas-Uber,[a] Leoní A. Barrios,[a,b] Olivier Roubeau,[c] and Guillem Aromí[a,b,*]

SUPPORTING INFORMATION

Contents

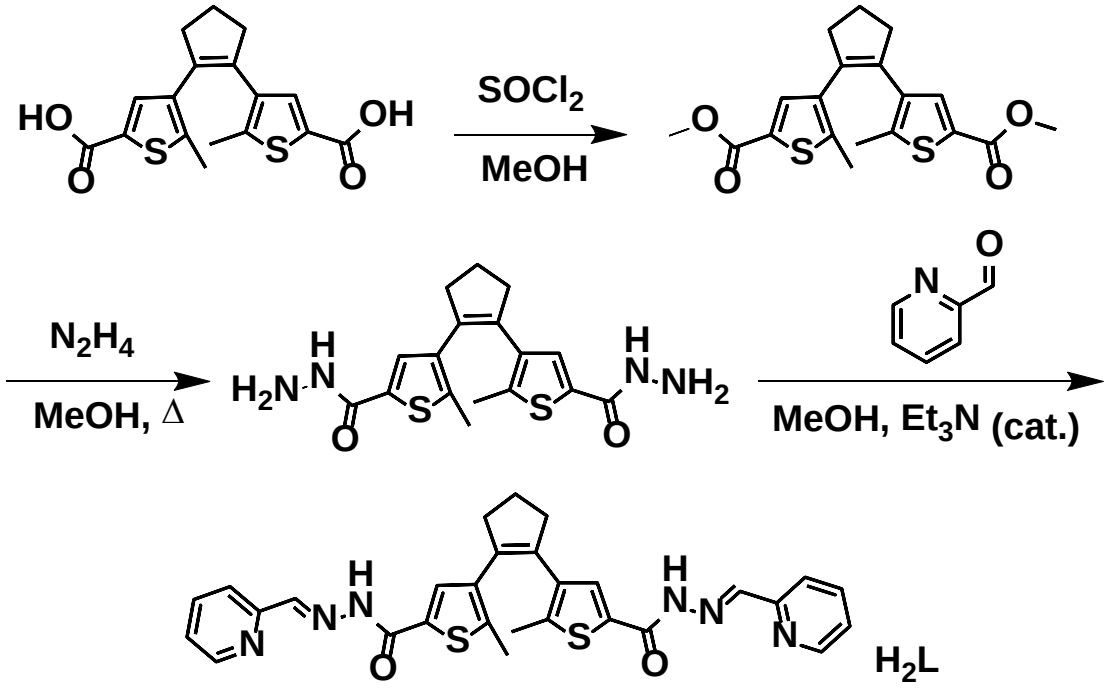

Scheme S1. Synthesis of H_2L.

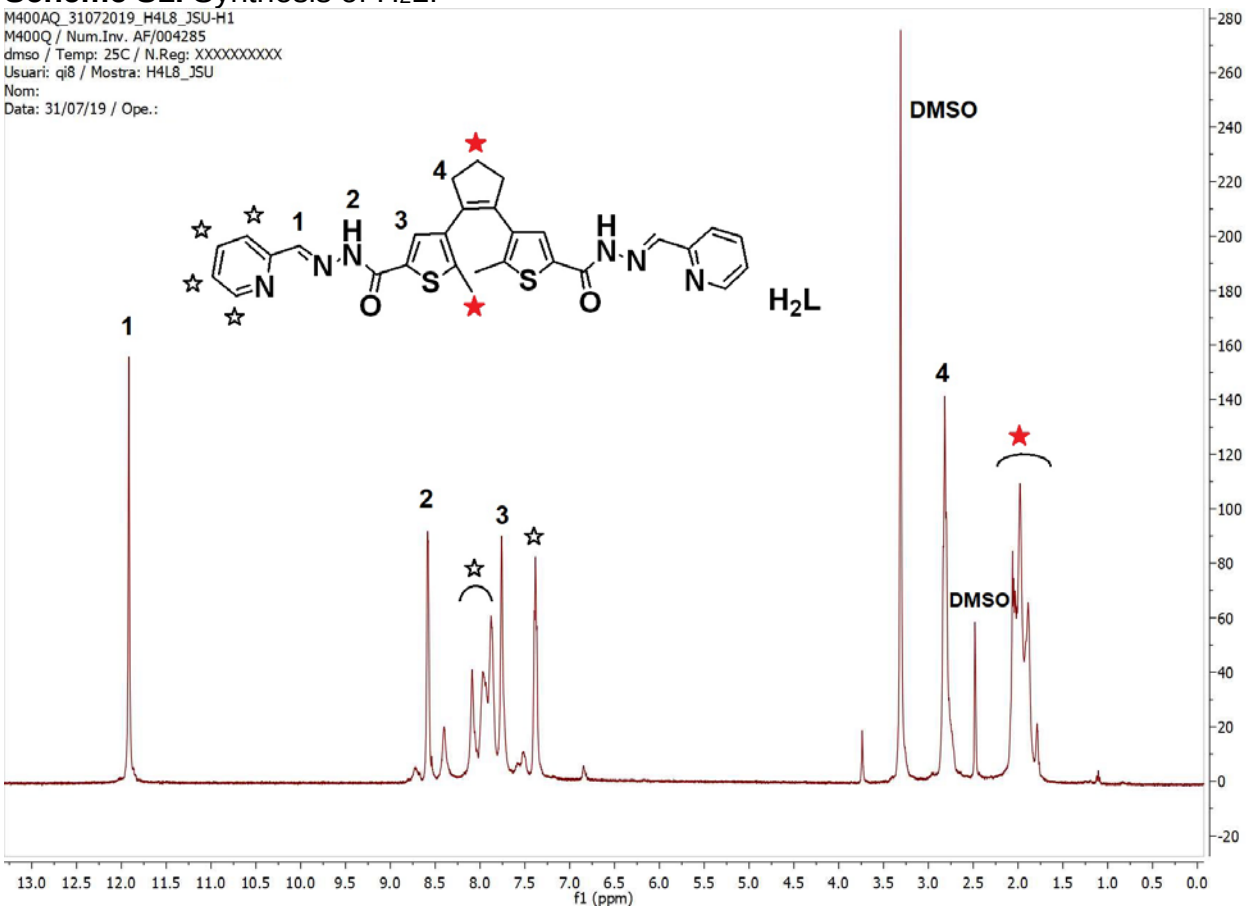

Figure S1. Assigned 400MHz ^{1}H NMR of H_2L in d_6-dmso.

Table S1. Crystallographic and refinement parameters for the structures of compounds **1** and **2**.

Compound	**1**	**2**
Formula	$C_{196}H_{186}Cl_4Dy_4N_{40}O_{13}S_8$	$C_{178}H_{174}Cl_4N_{36}O_{15}S_8Tb_4$
FW (g mol^{-1})	4358.12	4091.57
Wavelength (Å)	0.71073	0.7749
T (K)	150	100
Crystal system	tetragonal	tetragonal
Space group	$I4_1/a$	$I4_1/a$
a, b (Å)	36.8408(13)	36.8830(14)
c (Å)	14.8390(10)	14.7878(7)
V (Å^3)	20140(2)	20116.7(18)
Z	4	4
ρ_{calcd} (g cm^{-3})	1.437	1.350
μ (mm^{-1})	1.671	2.064
Reflections	7220	8314
R_{int}	0.0786	0.0231
Restraints	93	226
Parameters	442	528
S	1.058	1.040
R_1 [$I>2\sigma(I)$]	0.0798	0.0722
wR_2 [$I>2\sigma(I)$]	0.1783	0.1849
R_1 [all data]	0.1113	0.0913
wR_2 [all data]	0.1946	0.2065
Largest peak / hole (e Å^3)	1.183 / –0.738	1.661 / –1.662

Table S2. Intramolecular metal···metal separations and bond lengths (Å) describing the coordination environments of the metal sites in the structures of compounds **1** and **2**.

1		**2**	
Dy1–O1	2.268(7)	Tb1–O1	2.278(6)
Dy1–O2#1	2.330(7)	Tb1–O2#3	2.335(7)
Dy1–O3 *	2.412(19)	Tb1–O3 *	2.418(10)
Dy1–O4 *	2.42(2)	Tb1–O4 *	2.50(2)
Dy1–N1	2.591(10)	Tb1–N1	2.585(6)
Dy1–N2	2.484(9)	Tb1–N2	2.506(6)
Dy1–N5#1	2.533(9)	Tb1–N5#3	2.529(6)
Dy1–N6#1	2.615(9)	Tb1–N6#3	2.613(7)
Dy1–Cl1 *	2.686(8)	Tb1–Cl1 *	2.712(5)
Dy1–Cl2 *	2.723(9)	Tb1–Cl2 *	2.742(6)
Dy1···Dy1#1	9.612(4)	Tb1···Tb1#3	9.626(4)
Dy1···Dy1#2	10.724(4)	Tb1···Tb1#4	10.756(4)

* the coordinated water O3/O4 and chloride Cl1/Cl2 are mutually disordered over the 2 coordination sites

#1 = -y+3/4, x-1/4, -z+7/4; #2 = 1-x, -y+1/2, z

#3 = y-1/4, -x+5/4, -z+5/4; #4 = 1-x, -y+3/2, z

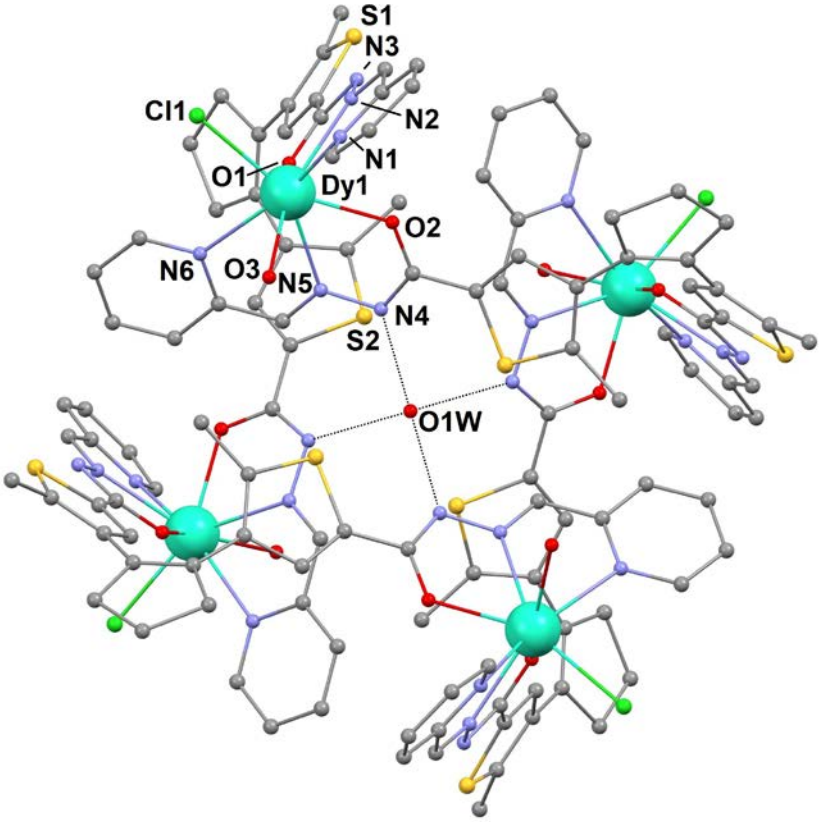

Figure S2. Molecular representation of $H_2O@[Dy_4L_4Cl_4(H_2O)_4]$ (**1**) with H-atoms omitted and crystallographically unique heteroatoms labelled. Only the main component of the disordered Cl / water terminal ligands is shown.

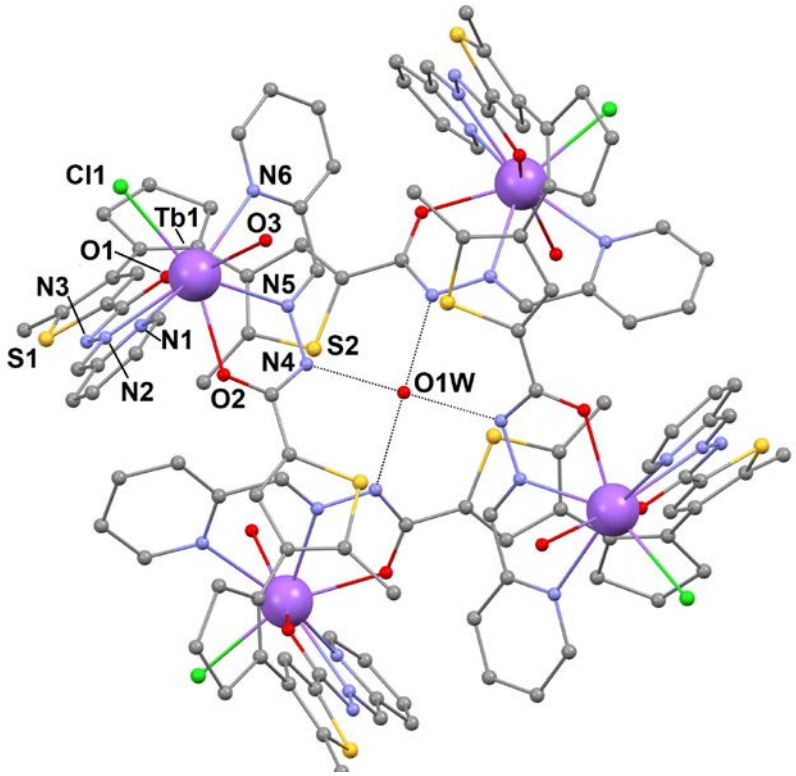

Figure S3. Molecular representation of $H_2O@[Tb_4L_4Cl_4(H_2O)_4]$ (**2**) with H-atoms omitted and crystallographically unique heteroatoms labelled. Only the main component of the mutually disordered Cl / water terminal ligands is shown.

Table S3. Distances and angles describing the hydrogen bonds in the structures of compounds **1** and **2**.

D–H···A	D–H (Å)	H···A (Å)	D···A (Å)	D–H···A (º)
1				
O1W–H1W···N4	0.95(2)	2.00(4)	2.898(8)	158(10)
2				
O1W–H1W···N4	0.95(2)	1.98(4)	2.886(6)	159(10)

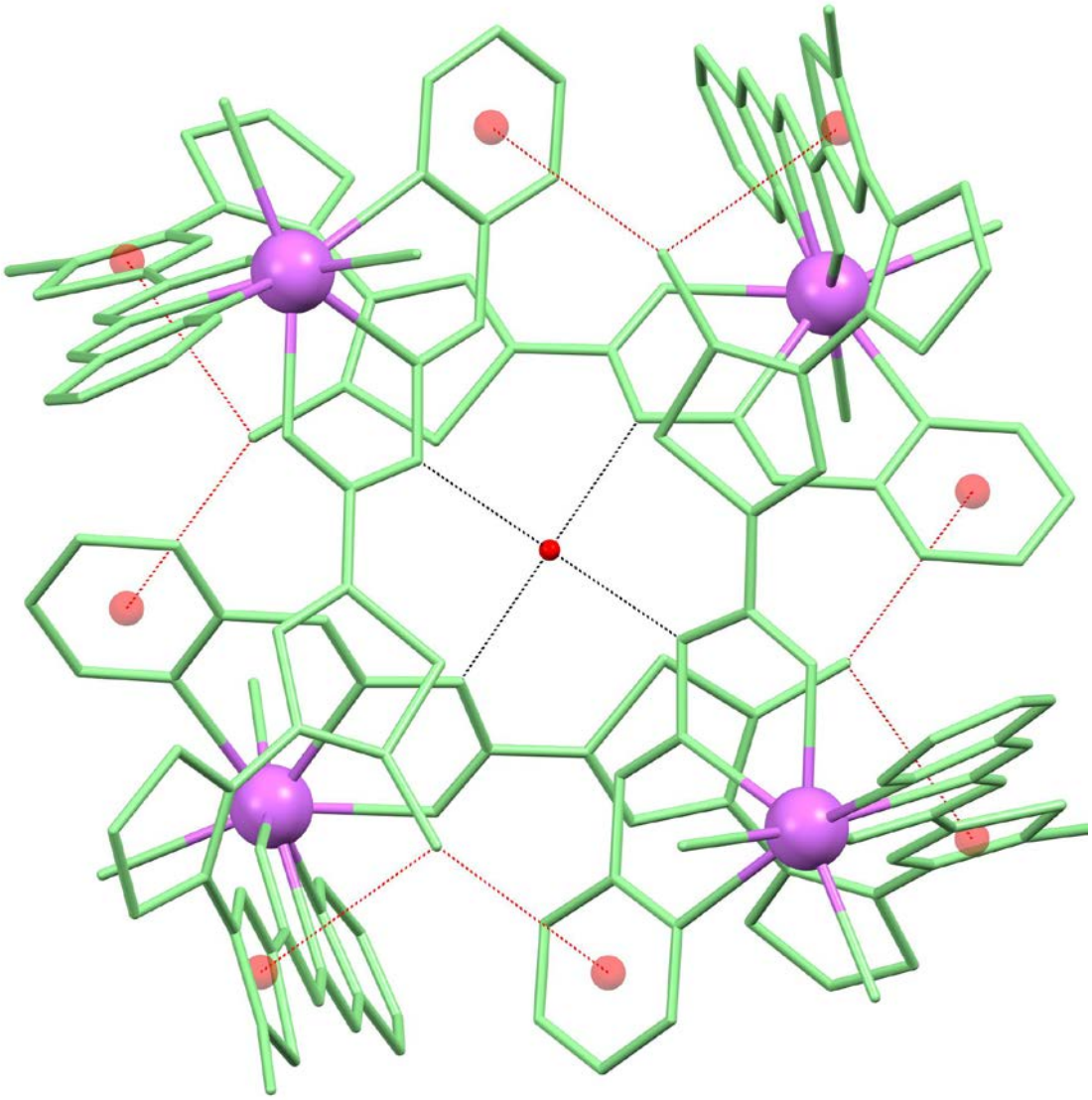

Figure S4. Representation of one unit of $H_2O@[Ln_4L_4Cl_4(H_2O)_4]$ (Ln=Dy, **1**; Tb, **2**) emphasizing the intramolecular hydrogen bonds (dashed black line) and C–H···π interactions (dashed red line). The centroids involved in the latter are represented as faded red spheres.

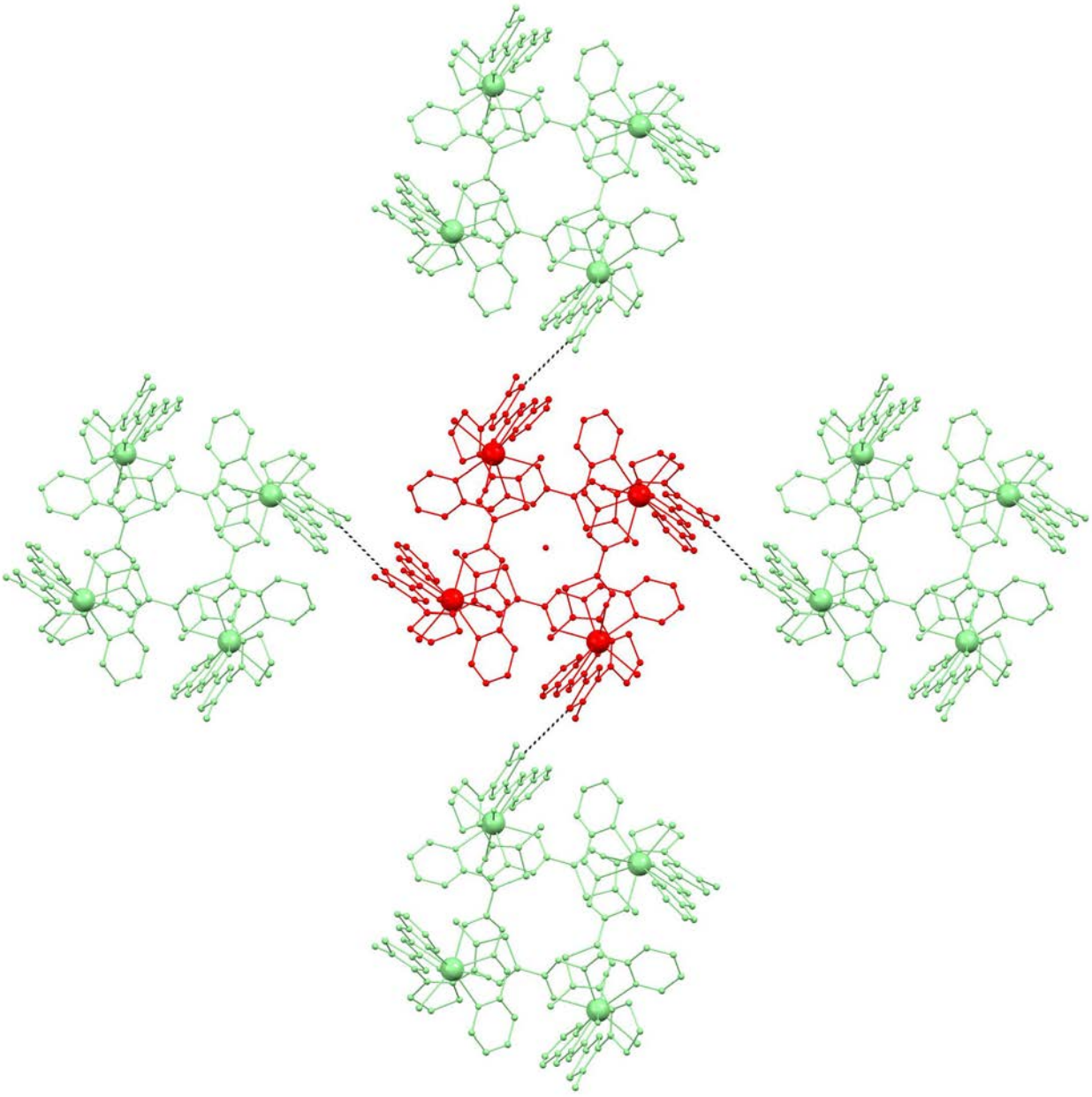

Figure S5. Representation of one unit of $H_2O@[Ln_4L_4Cl_4(H_2O)_4]$ (red; Ln=Dy, **1**; Tb, **2**) surrounded by its four first neighbours (green) *via* S···S interactions (marked as dashed lines), viewed along the crystallographic *c* axis.

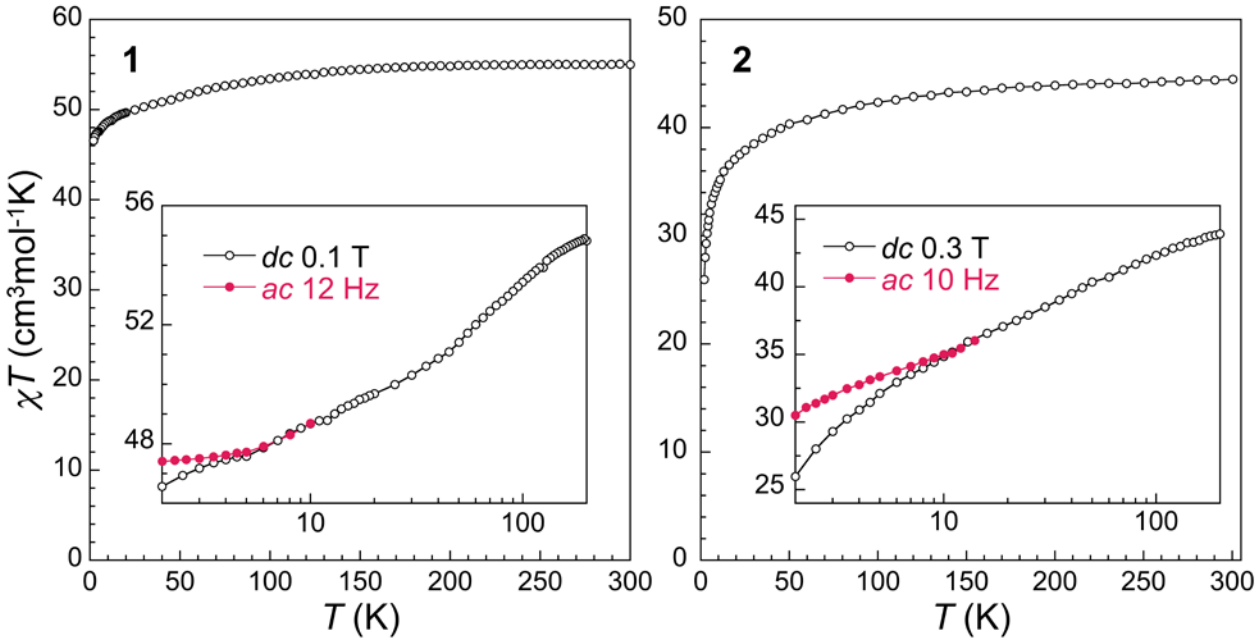

Figure S6. Temperature dependence of the χT product (χ is the molar paramagnetic susceptibility) for compounds **1** (left) and **2** (right), as derived from *dc* measurements under an applied *dc* field of respectively 0.1 and 0.3 T. Insets are semi-logarithmic plots in the 2-200 K range, superimposed to the equilibrium susceptibility derived from zero-field *ac* measurements at low frequencies. The differences point at dynamics of the magnetization under applied fields.

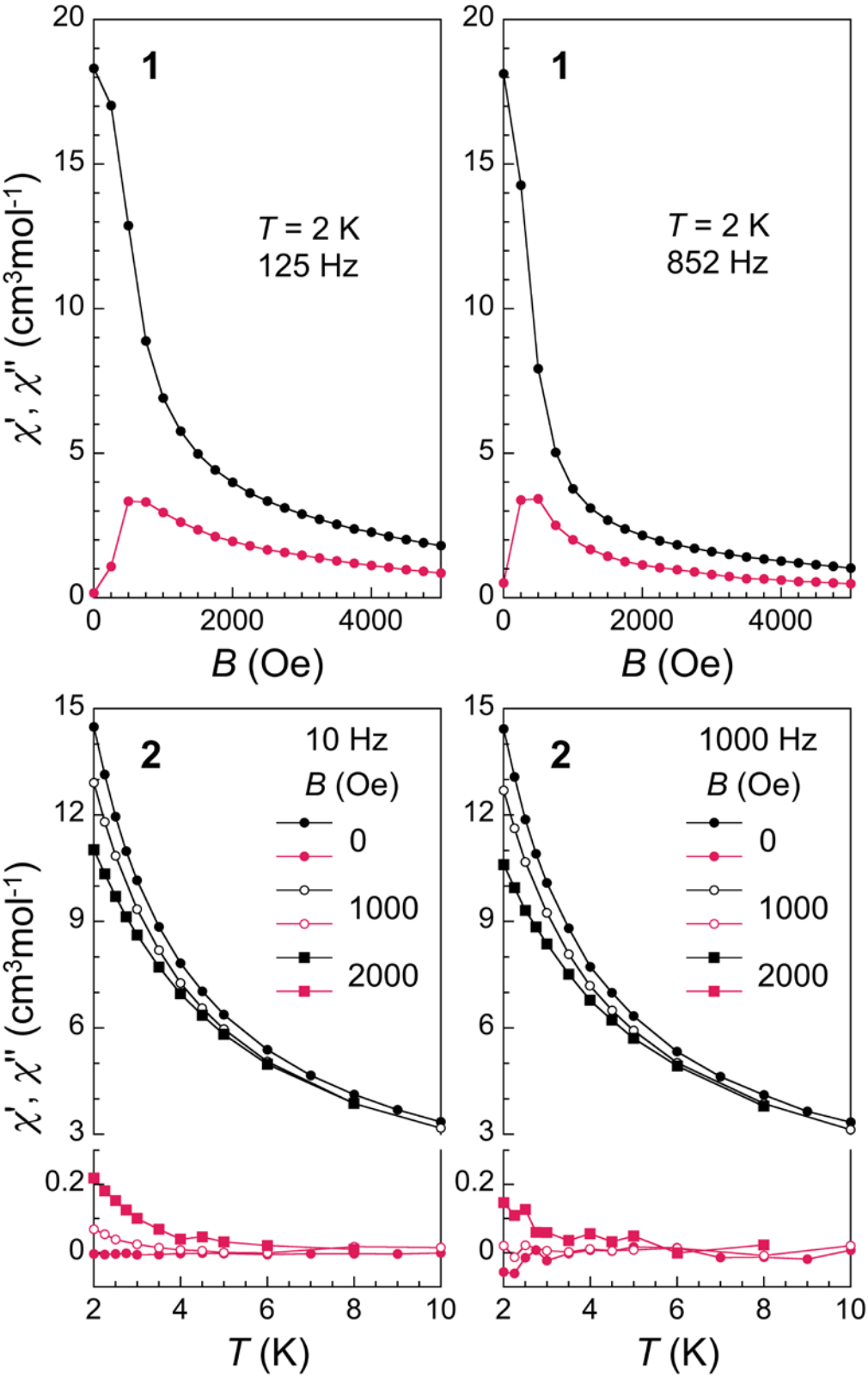

Figure S7. Preliminary evaluation of the magnetization slow dynamics in **1** (top) and **2** (bottom): real and imaginary *ac* susceptibilities, χ' (black symbols) and χ'' (red symbols), at variable fields and two frequencies at 2 K in the case of **1**, and at variable temperature and three fields and two frequencies in the case of **2**, as indicated.

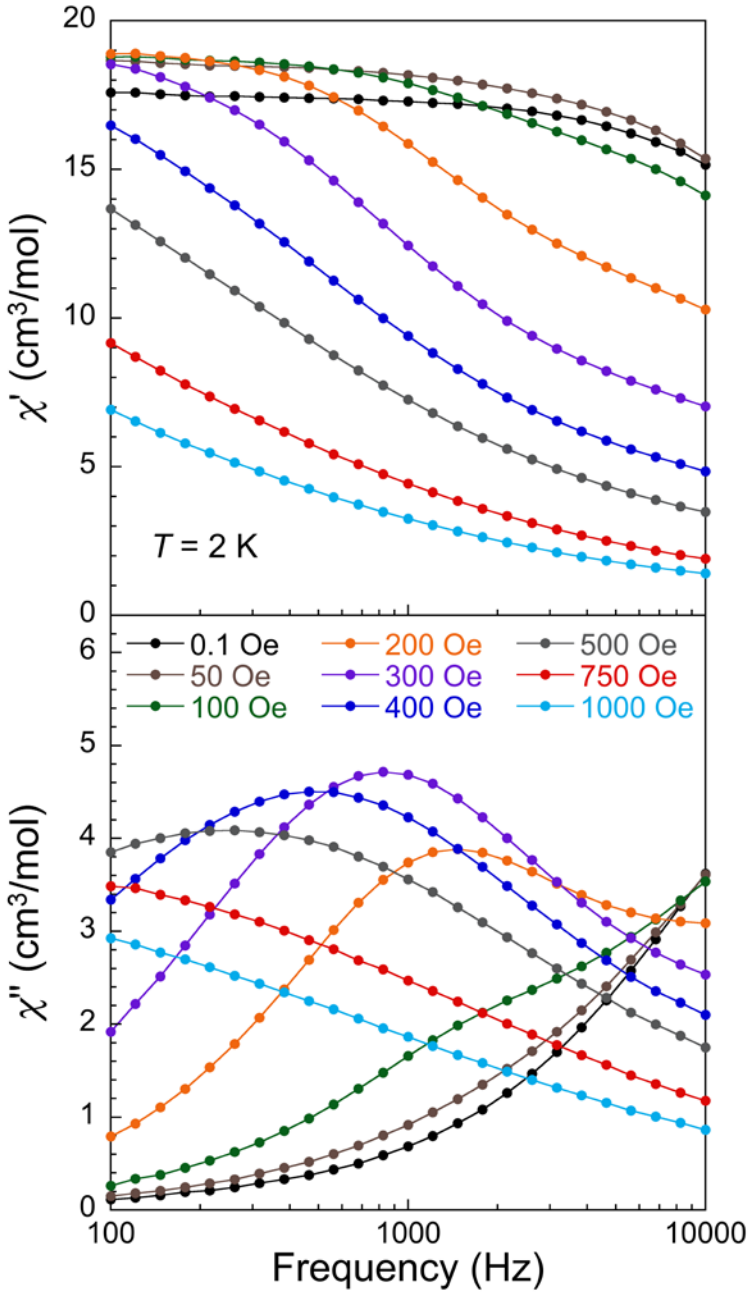

Figure S8. Frequency dependence of the in-phase (top) and out-of-phase (bottom) *ac* magnetic susceptibility of **1** at 2 K and under increasing applied *dc* fields as indicated. Lines are only guides to eye.

The data were fitted to the corresponding generalized Debye model expressions:

$$\chi'(\omega) = \chi_S + (\chi_T - \chi_S)\frac{1 + (\omega\tau)^{\beta}\cos\left(\frac{\pi\beta}{2}\right)}{1 + 2(\omega\tau)^{\beta}\cos\left(\frac{\pi\beta}{2}\right) + (\omega\tau)^{2\beta}}$$

$$\chi''(\omega) = (\chi_T - \chi_S)\frac{(\omega\tau)^{\beta}\sin\left(\frac{\pi\beta}{2}\right)}{1 + 2(\omega\tau)^{\beta}\cos\left(\frac{\pi\beta}{2}\right) + (\omega\tau)^{2\beta}}$$

in which τ is the magnetization relaxation time, ω is the angular frequency, χ_T the isothermal susceptibility, χ_S the adiabatic susceptibility and β describes the distribution of relaxation times.

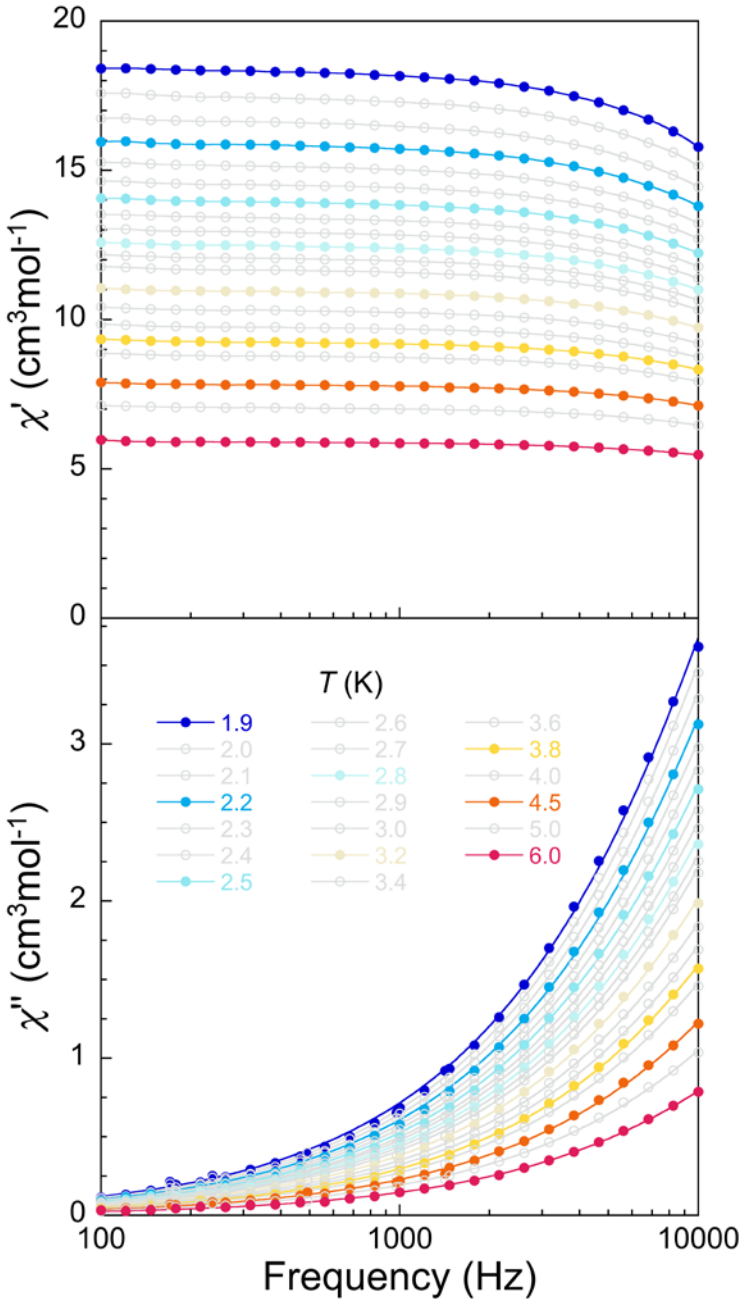

Figure S9. Frequency dependence of the in-phase (top) and out-of-phase (bottom) *ac* magnetic susceptibility of **1** at zero *dc* field and increasing temperatures as indicated. Lines are fits of the experimental data to the generalized Debye model expressions for the real and imaginary susceptibility (see caption of Fig. S7). β was fixed at the same value of 0.78 for all temperatures, to avoid over parameterization.

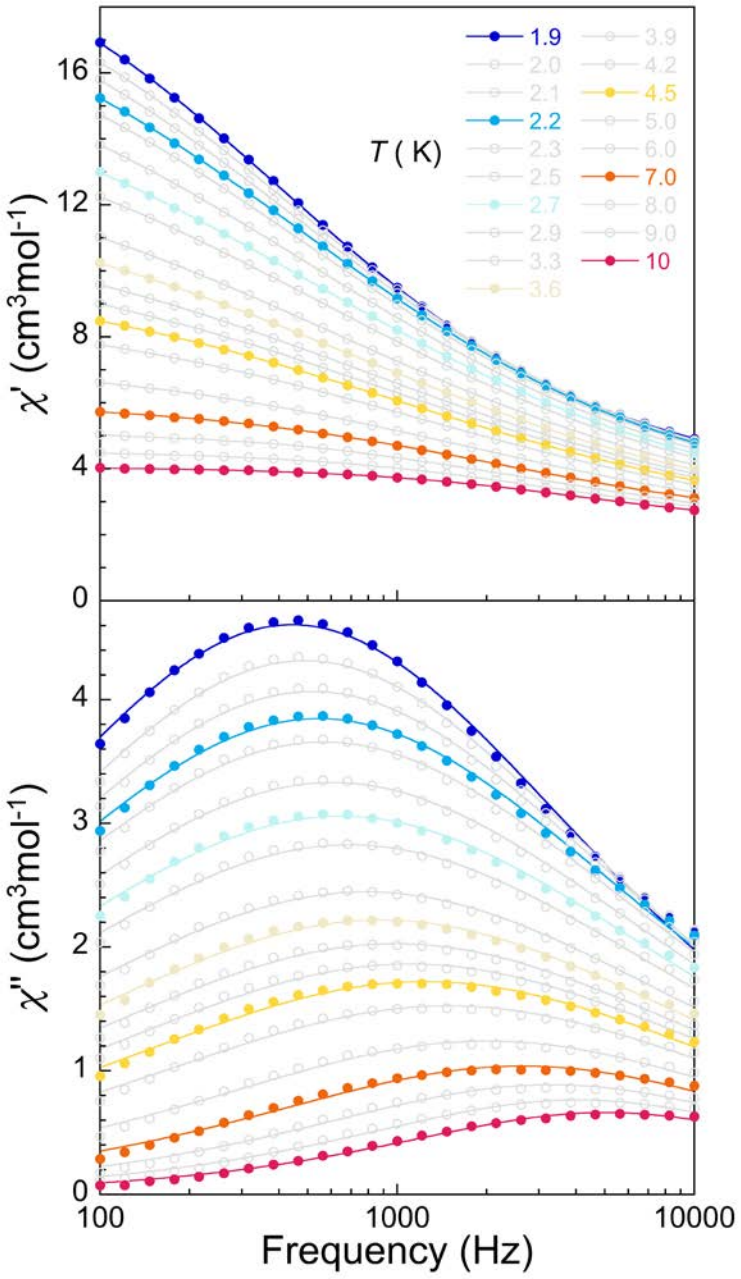

Figure S10. Frequency dependence of the in-phase (top) and out-of-phase (bottom) *ac* magnetic susceptibility of **1** at 400 Oe and increasing temperatures as indicated. Lines are fits of the experimental data to the Generalized Debye model expressions for the real and imaginary susceptibility (see caption of Fig. S7). β remained in the range 0.53-0.75, and the derived values of τ were in good agreement with those obtained considering the relation $\tau = (2\pi\nu_{max})^{-1}$ with ν_{max} the frequency at which χ'' is maximum.

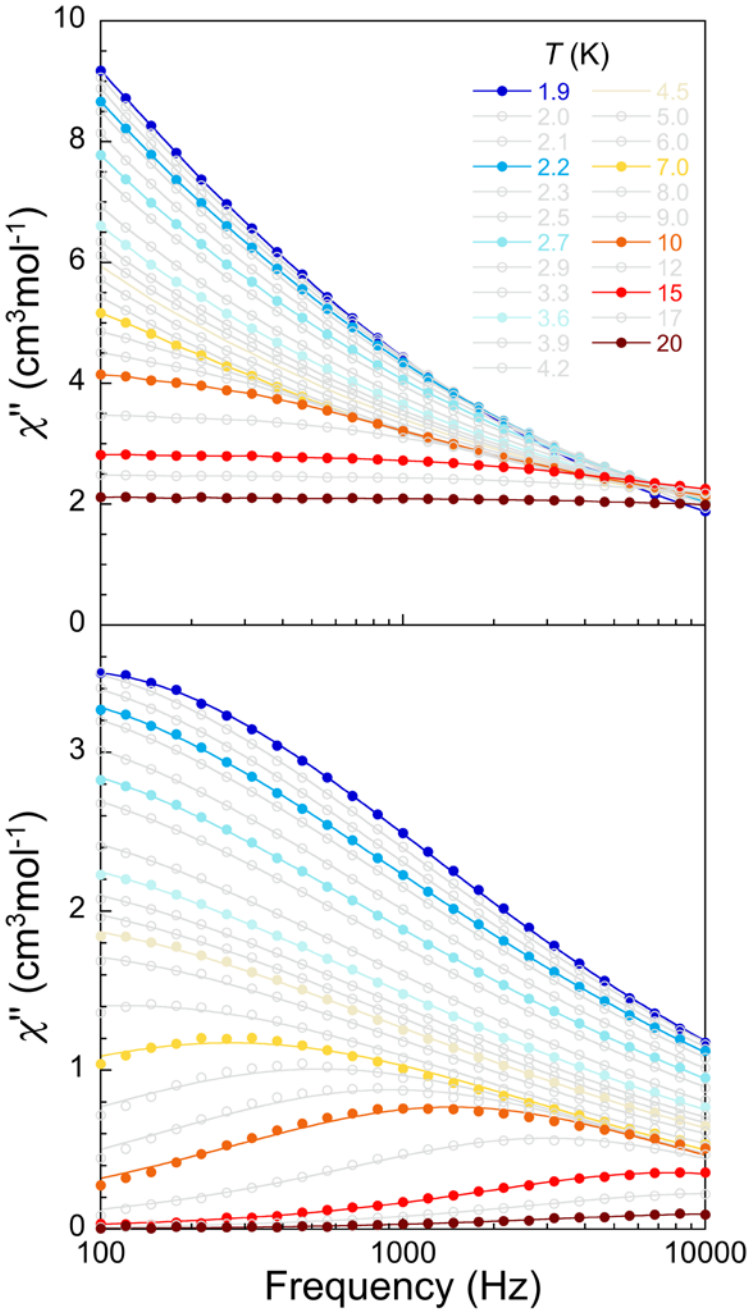

Figure S11. Frequency dependence of the in-phase (top) and out-of-phase (bottom) *ac* magnetic susceptibility of **1** at 750 Oe and increasing temperatures as indicated. Lines are fits of the experimental data to the Generalized Debye model expressions for the real and imaginary susceptibility (see caption of Fig. S7). The derived values of τ were in good agreement with those obtained considering the relation $\tau = (2\pi\nu_{max})^{-1}$ with ν_{max} being the frequency at which χ'' is maximum, while β remained in the range 0.50-0.78 when the maximum in χ'' was in the experimental frequency window. When not, *i.e.* at temperatures lower than 5 K and at 17 and 20 K, large errors on τ are estimated with β taking values between 0.4 and 0.5 for T < 5 K (β was fixed at 0.79 for T = 17 and 20 K).